Carbonate ion concentrations, ocean carbon storage and atmospheric CO_2

22nd May 2013

Philip Goodwin[1] and Jonathan Maitland Lauderdale[2]

[1]*Department of Earth Sciences, University of Cambridge, Downing Street, Cambridge, CB2 3EQ, UK*

[2] *School of Environmental Sciences, University of Liverpool, Nicholson Building, Liverpool, L69 3GP, UK*

Goodwin, P. and J.M. Lauderdale (2013) Carbonate ion concentrations, ocean carbon storage and atmospheric CO_2, *Global Biogeochemical Cycles*, 27, doi:10.1002/gbc.20078. To view the open abstract, go to http://dx.doi.org and enter the DOI.

Abstract

Reconstructing past-ocean [CO_3^{2-}] allows the paleo-depth of the chemical lysocline to be constrained, an important control on past atmospheric CO_2. However, the causal mechanisms responsible for observed spatial and temporal variation in [CO_3^{2-}] are difficult to quantify because of the complicated carbonate chemistry system. Here, spatial and temporal variations in [CO_3^{2-}] are quantitatively and concisely related to variations in ocean carbon storage due to different processes. The spatial variation in [CO_3^{2-}] is given by $\Delta[CO_3^{2-}]=\gamma(\Delta C_{soft}+\Delta C_{dis}+(\partial C_{sat}/\partial T)\Delta T-\Delta C_{carb})$, where C_{soft} and C_{carb} are the DIC from remineralisation of marine soft-tissue and $CaCO_3$ respectively, T is seawater temperature, $(\partial C_{sat}/\partial T)$ is the temperature-solubility sensitivity of DIC, C_{dis} is the DIC from air-sea disequilibrium and γ is a carbonate-chemistry coefficient. A similar quantitative function for temporal variation in global mean-ocean [CO_3^{2-}] is derived in terms of atmospheric CO_2, $CaCO_3$ precipitation and dissolution, and carbon exchanges of terrestrial or fossil fuel origin. Comparing published [CO_3^{2-}] reconstructions at the Last Glacial Maximum (LGM) and late Holocene, the quantitative relationships reveal how the spatial distribution of ocean carbon storage was altered. Relative to the Intermediate North Atlantic the rest of the ocean saw $C_{soft}+C_{dis}+(\partial C_{sat}/\partial T)T-C_{carb}$ increase by an extra 570 to 970PgC during LGM. Assuming Intermediate North Atlantic $C_{soft}+C_{dis}+(\partial C_{sat}/\partial T)T-C_{carb}$ did not decrease during the LGM, this 570 to 970PgC increase in the rest of the ocean is enough to explain 40 to 70% of the observed glacial decrease in atmospheric CO_2.

1. Introduction

Ocean carbonate ion concentrations, $[CO_3^{2-}]$, are intricately linked to atmospheric CO_2 levels and climate via ocean carbonate chemistry [*Ridgwell and Zeebe*, 2005]. Many methods are used to reconstruct past ocean $[CO_3^{2-}]$: a $CaCO_3$ grain size index [*Chiu and Broecker*, 2008]; the percentage-weight of carbonate in sediments [*Hoddell et al*, 2001]; and trace metal ratios in foraminifera, such as Mg/Ca [*Elderfield et al*, 2006] and B/Ca [*Yu and Elderfield*, 2007].

Reconstructing past-ocean $[CO_3^{2-}]$ can locate changes to the depth of the calcite saturation horizon due to the inverse relationship between the saturation-state of $CaCO_3$ and $[CO_3^{2-}]$ [see *Ridgwell and Zeebe*, 2005 and references therein]. Through examining the time evolution of the calcite saturation horizon, and the closely associated chemical lysocline, transient $CaCO_3$ dissolution or preservation events can be identified. Both the past calcite saturation horizon depth, and temporal $CaCO_3$ dissolution or preservation events, reveal significant information about past ocean carbon cycling and the causes of changing atmospheric CO_2 [*Broecker*, 1982a; 1982b; *Archer*, 1991; *Marchitto et al*, 2005; *Sigman et al*, 1998; *Sigman and Boyle*, 2000].

Goodwin et al [2008] present an analytical model showing how atmospheric CO_2, P_{CO2} (parts per million by volume, ppm), varies on millennial timescales with simultaneous perturbations to up to 5 global variables:
(1) Carbon added to the air-sea system though global imbalances in 'open-system' $CaCO_3$ sedimentation and dissolution, ΔI_{open} (PgC), [*Goodwin et al*, 2008];
(2) Charge neutral carbon removed from the air-sea system through an increase in terrestrial carbon storage, ΔI_{ter}, or carbon emitted to the system from fossil fuels, ΔI_{em} (PgC) [*Goodwin et al*, 2008];
(3) Increased global mean ocean DIC concentration due to regenerated soft tissue, ΔC_{soft} (moles C m^{-3}) [*Marinov et al*, 2008; *Goodwin et al*, 2008; *Ito and Follows*, 2005], where C_{soft} is the remineralised phosphate concentration multiplied by the ratio of carbon to phosphate in organic matter [*Sarmiento and Gruber*, 2006; *Williams and Follows*, 2011];
(4) Increased DIC concentrations due to regenerated hard tissue, ΔC_{carb} (moles C m^{-3}) [*Goodwin et al*, 2008], where C_{carb} is the half the increase in sub-surface alkalinity from the remineralisation of $CaCO_3$ hard tissue [*Sarmiento and Gruber*, 2006; *Williams and Follows*, 2011]; and
(5) Increased ocean disequilibrium of DIC with atmospheric CO_2, ΔC_{dis} (moles C m^{-3}), where C_{dis} is equivalent to the C_{res} term of *Williams and Follows* [2011] and the $\Delta C_{dis\ eq}$ term of *Gruber et al* [1996]. It should be noted that alterations to C_{soft}, C_{carb} and T may all lead to an alteration in C_{dis}, therefore C_{dis} captures the air-sea gas exchange components of the biological and solubility carbon pumps.
Recent studies have also shown how P_{CO2} on millennial timescales relates to a 6th global variable: (6) Increased global mean ocean temperatures, ΔT (K), [*Omta et al*, 2011; *Goodwin et al*, 2011].

$[CO_3^{2-}]$ is approximated by the difference between titration alkalinity, A_T, and dissolved inorganic carbon, DIC: $[CO_3^{2-}] \sim A_T\text{-}DIC$. It is thus well known that the spatial distribution of $[CO_3^{2-}]$ is explained by considering the distributions of C_{soft}, C_{carb}, C_{dis} [*Sarmineto and Gruber*, 2006] and T [*Omta et al*, 2011], and also that changes to P_{CO2}, ΔI_{ter} and ΔI_{open} alter $[CO_3^{2-}]$ over time. Concise formalistic relations linking spatial and temporal changes in ocean carbon storage to the observed changes in reconstructed $[CO_3^{2-}]$ have proved elusive, due to the complicated ocean carbonate chemistry system. This study presents compact formalistic

relationships showing how $[CO_3^{2-}]$ varies quantitatively with 7 terms: ΔP_{CO2}, ΔI_{open}, ΔI_{ter}, ΔT, ΔC_{soft}, ΔC_{dis}, and ΔC_{carb}. The analytical relations are derived in sections 2 to 4, and tested against two numerical models that each contain explicit numerical solutions of the carbonate chemistry system. Section 5 applies the new relationships to quantify changes in ocean carbon cycling between the Holocene and Last Glacial Maximum (LGM) implied by the $[CO_3^{2-}]$ reconstructions of *Yu et al* [2010]. Section 6 then discusses the broader implication of the study.

2. Analytical relationships between ocean processes and temporal and spatial variations in $[CO_3^{2-}]$

Carbonate alkalinity, A_C, and DIC are defined in terms of the concentrations of carbonate species,

$$A_C = [HCO_3^-] + 2[CO_3^{2-}], \quad (1)$$

and

$$C_{DIC} = [CO_2^*] + [HCO_3^-] + [CO_3^{2-}]. \quad (2)$$

Consider what happens to $[CO_3^{2-}]$ in a surface water parcel initially in chemical equilibrium with the atmosphere if A_C and P_{CO2} are altered. C_{DIC} will change due to air-sea flux of CO_2 until a new chemical equilibrium is reached. The change in $[CO_2^*]$ is determined by the change in P_{CO2}, because $[CO_2^*]$ is proportional to P_{CO2} for a water parcel at chemical equilibrium assuming constant temperature and salinity. From (1) and (2) the change in $[CO_3^{2-}]$ is given by the change in A_C-C_{DIC} plus the change in $[CO_2^*]$,

$$\Delta[CO_3^{2-}] = \Delta(A_C - C_{DIC}) + \Delta[CO_2^*]. \quad (3)$$

However, it is more useful to consider A_T, than A_C, because A_T is a conserved tracer. A_T is larger than (but closely approximated by) A_C, allowing (3) to be re-written in terms of A_T,

$$\Delta[CO_3^{2-}] = \gamma\Delta(A_T - C_{DIC}) + \Delta[CO_2^*], \quad (4)$$

where γ is a coefficient defined as $\gamma = \Delta(A_C - C_{DIC})/\Delta(A_T - C_{DIC})$. A value of γ=1 would indicate that $\Delta A_T = \Delta A_C$ at the surface ocean, and γ<1 indicates that $|\Delta A_T| > |\Delta A_C|$. In applying (4), it is assumed that a uniform value for γ applies across the entire ocean. Focussing on (4), $\Delta[CO_3^{2-}]$ is now related to variations in ocean carbon storage.

2.1 Spatial variations in $[CO_3^{2-}]$

2.1 Theory

Local total DIC concentration is the sum of components due to different processes [*Ito and Follows*, 2005],

$$C_{DIC} = C_{sat} + C_{dis} + C_{soft} + C_{carb}, \quad (5)$$

where C_{sat} is the DIC concentration of the water parcel if brought into chemical equilibrium with the overlying atmospheric CO_2 concentration, C_{dis} is the disequilibrium concentration at the time of subduction from the surface mixed layer (i.e. the difference between C_{DIC} and C_{sat} at subduction), C_{soft} is the concentration of DIC due to the regeneration of soft tissue organic carbon, and C_{carb} is the DIC concentration due to dissolved $CaCO_3$ hard tissue. Similarly, A_T has a preformed component and a component from dissolved marine $CaCO_3$ hard-tissue material,

$$A_T = A_{pre} + A_{carb}, \quad (6)$$

where this ignores the smaller contribution to A_T from nitrate in remineralised soft tissue. Substituting (5) and (6) into (4) gives $\Delta[CO_3^{2-}]$ in terms of the change in component concentrations of A_T and C_{DIC} from each process,

$$\Delta[CO_3^{2-}] = \gamma\Delta\left(A_{pre} + A_{carb} - C_{sat} - C_{soft} - C_{dis} - C_{carb}\right), \quad (7)$$

where the $\Delta[CO_2^*]$ term in (4) is assumed to be negligible. This assumption is reasonable since $[CO_2^*]$ varies in the present ocean by order 20μmol kg^{-1} between ocean basins, whereas $[CO_3^{2-}]$ varies by order 130μmol kg^{-1} [*Sarmiento and Gruber*, 2006]. The total change in C_{sat} is split into contributions from T, A_T and P_{CO2} [*Goodwin and Lenton*, 2009],

$$\Delta C_{sat} = \left.\frac{\partial C_{sat}}{\partial A}\right|_{T,P_{CO2}} \Delta A_{pre} + \left.\frac{\partial C_{sat}}{\partial T}\right|_{A_T,P_{CO2}} \Delta T + \left.\frac{\partial C_{sat}}{\partial P_{CO2}}\right|_{A_T,T} \Delta P_{CO2}, \quad (8)$$

where a minor contribution from salinity has been ignored. Substituting (8) into (7), noting again that ΔP_{CO2}=0 when considering spatial variation in the ocean, gives

$$\Delta[CO_3^{2-}] = \gamma\left(\Delta A_{pre} + \Delta A_{carb} - \left.\frac{\partial C_{sat}}{\partial A_T}\right|_{T,P_{CO2}} \Delta A_{pre} - \left.\frac{\partial C_{sat}}{\partial T}\right|_{A_T,P_{CO2}} \Delta T - \Delta C_{soft} - \Delta C_{dis} - \Delta C_{carb}\right). \quad (9)$$

Equation (9) is simplified noting that: C_{sat} increases in an approximate 1:1 ratio with A_T at fixed T and P_{CO2}, $\left.\frac{\partial C_{sat}}{\partial A_T}\right|_{T,P_{CO2}} \approx 1$; and $CaCO_3$ dissolution increases A_{carb} by 2 moles per 1 mole increase in C_{carb}, $\Delta A_{carb} = 2\Delta C_{carb}$, leaving

$$\Delta[CO_3^{2-}] = -\gamma\left(\frac{\partial C_{sat}}{\partial T}\Delta T + \Delta C_{soft} + \Delta C_{dis} - \Delta C_{carb}\right), \quad (10)$$

where $\left.\frac{\partial C_{sat}}{\partial T}\right|_{A_T,P_{CO2}} \approx -0.01$ moles C m^{-3}K^{-1} in seawater [*Goodwin and Lenton*, 2009]. This relationship (10) predicts how $[CO_3^{2-}]$ varies spatially in the ocean in terms of variations in ocean temperature and DIC concentrations due to different processes. The timescales over which equation (10) is valid is determined by the assumption that the ΔP_{CO2} term in (8) can be ignored. Assuming ΔP_{CO2}=0 in (8) implies that C_{sat} is calculated relative the same P_{CO2} level for the whole ocean. Thus, (10) is valid when P_{CO2} does not change significantly over the timescale of ocean overturning, circa 1000 years.

2.2 Numerical Model Comparisons

This section tests the predicted relationship for spatial variations in $[CO_3^{2-}]$, (10), against two numerical ocean models: the Isopycnal Box Model [*Goodwin,* 2012] and the Massachusetts Institute of Technology General Circulation Model (MITgcm) [*Marshall et al*, 1997]. Both models contain explicit numerical solutions of the carbonate chemistry system after *Follows et al* [2006], including the impacts of the boric buffer system. The MITgcm also includes the impact of soft tissue nitrate remineralisation on A_T, which is ignored in the Isopycnal Box Model. Thus, the numerical model comparisons constitute a suitable test of the carbonate chemistry assumptions used in the analytical derivation, (1) to (10).

2.2.1 Isopycnal Box Model comparison

The Isopycnal Box Model [*Goodwin*, 2012] comprises a number of isopycnal slabs each with prescribed potential density, which are vertically stacked in density order with the densest slabs at the bottom (Fig. 1). Each isopycnal slab is split into three boxes; a sub-surface box, and surface boxes in the northern and southern hemispheres (Fig. 1). Sea surface buoyancy fluxes are prescribed and the circulation consists of diapycnal volume fluxes and diapycnal diffusion between the boxes, and isopycnal volume fluxes from the surface mixed layer to the sub-surface ocean [*Goodwin*, 2012]. The model is configured with 29 isopycnal slabs ranging

in density from 1028.23kg m^{-3} to 1023.92kg m^{-3}. An idealized preindustrial circulation is applied, and parameters representing diapycnal diffusivity are tuned to accurately reproduce the fraction of the global ocean ventilated through each surface region [*Goodwin*, 2012 – figures 6 and 13 therein].

Here, a representation of the ocean carbon cycle is coupled to the model, including air-sea exchange of CO_2 and biological uptake of nutrients and carbon in the euphotic zone, with export and remineralisation to depth (Fig. 1). A uniform salinity of 35psu is imposed, and the potential temperatures of the boxes are then calculated from their prescribed potential densities at this salinity after *Fofonoff* [1985] (Fig. 2). The Isopycnal Box Model solves for the biogeochemical tracer concentrations of A_T, phosphate, DIC, preformed A_T, preformed phosphate and C_{sat}. These tracers are advected and diffused using the volume fluxes and diffusivities calculated for the physical model [*Goodwin*, 2012]. The speciation of DIC (2) and its air-sea exchange is calculated as a function of local tracer values after *Follows et al* [2006]. The ratio of carbon to phosphate in falling Particulate Organic Carbon (POC) is set to 105, and the rain ratio of $CaCO_3$ to organic carbon leaving the euphotic zone is 0.1. The export flux of POC leaving the euphotic zone in each surface box, $F_{POC}(z_c)$ (Fig. 1), is set to restore surface phosphate concentrations to prescribed values, initially set here to 1.0×10^{-3} moles m^{-3} across the surface ocean. Remineralisation of POC vertically below each surface ocean box is calculated using a power law after *Martin et al* [1987],

$$F_{POC}(z) = F_{POC}(z_c)\left(\frac{z}{z_c}\right)^b, \qquad (11)$$

where $F_{POC}(z)$ is the flux of POC at depth z, z_c is the euphotic zone depth set here to 75m, and the exponent b is set to 1.0. Remineralisation of falling $CaCO_3$ occurs using an exponential remineralisation depth-scale of 3500m. Any falling POC and $CaCO_3$ arriving in the deepest box is remineralised, with no sediment accumulation. The initial uniform C_{DIC}, A_T and phosphate concentrations are set to 2.1moles m^{-3}, 2.35moles m^{-3}, and 2.3×10^{-3}moles m^{-3} respectively. The ocean model is then coupled to an atmospheric box with a fixed prescribed P_{CO2} of 280ppm and air-sea exchange of CO_2 is permitted with a fixed air-sea gas transfer coefficient (Table 1). The model is spun up for over 13000 years, using a time-step of 1 day, until ocean DIC stabilises. The model parameter values used in the spin-up are given in Table 1.

The analytical prediction (10) is then tested considering spatial variation in $[CO_3^{2-}]$ compared to the sub-surface box with potential density 1026.4kg m^{-3}, which has an equatorial depth of 156m. This sub-surface box has an ambient $[CO_3^{2-}]$=89.6 mmol m^{-3}, and defines $\Delta[CO_3^{2}]$ $=\Delta T=\Delta C_{soft}=\Delta C_{dis}=\Delta C_{carb}=0$. This location is chosen because the ambient $[CO_3^{2-}]$ is not an extreme value relative to the rest of the model ocean (Fig. 3a, b and c). The stabilised DIC component concentrations are identified (Fig. 2). C_{DIC} and C_{sat} are carried as tracers in the model (Fig. 2a, black and grey respectively). C_{soft} is calculated using the difference between total phosphate and preformed phosphate [*Ito and Follows*, 2005] (Fig. 2b, black dots and solid line) and C_{carb} is similarly calculated using the difference between total A_T and preformed A_T (Fig. 2b, grey dots and solid line). C_{dis} is then calculated as the contribution not attributable to other mechanisms, $C_{dis}=C_{DIC}-C_{sat}-C_{soft}-C_{carb}$ (Fig. 2b, black crosses and dashed line). To evaluate the $\frac{\partial C_{sat}}{\partial T}\Delta T$ term in (10), a value of $\left.\frac{\partial C_{sat}}{\partial T}\right|_{A_C,P_{CO2}} \approx -0.01$ moles C $m^{-3}K^{-1}$ [*Goodwin and Lenton*, 2009] is used along with the potential temperature profile (Fig. 2c).

The value of γ is calculated by plotting $[CO_3^{2-}]$ against A_T-C_{DIC} across the surface ocean (4), and assuming $\Delta[CO_3^{2-}] >> \Delta[CO_2^*]$. The gradient of observed linear relationship shows that γ is approximately uniform across the model surface ocean, at a value of γ=0.64 (Fig. 4a). The analytical relation (10) accurately predicts $[CO_3^{2-}]$ for the majority of ocean boxes (Fig. 4b). The spatial variation in $[CO_3^{2-}]$ is accurately predicted for most of the deep and surface ocean (Fig. 3). For the Isopycnal Box Mode spin up, the largest source of error in the prediction (10) occurs at surface locations with high potential density (Fig. 3e,f), which have the lowest ambient surface $[CO_3^{2-}]$ (Fig. 3b,c).

2.2.2 General Circulation Model comparison

The MITgcm [*Marshall et al*, 1997] is globally configured at coarse resolution (2.8°x2.8°) in the horizontal with 15 non-uniform vertical levels. The model is forced with monthly-mean cycles of heat, freshwater [*Jiang et al*, 1999] and wind stress [*Trenberth et al*, 1989], and contains coupled biogeochemistry [*Dutkiewicz et al*, 2005; *Parekh et al*, 2005]. The model is spun up reaching a steady state P_{CO2} of 278.05 ppm. A full description of the model configuration and spin-up are found in *Lauderdale et al* [2013] and references therein.

The analytical prediction (10) is then assessed considering spatial variation in $[CO_3^{2-}]$ compared to an arbitrary location, just below the pycnocline in the Pacific sector of the Southern Ocean (142°W, 43.5°S and 1250 m depth). In the MITgcm spin-up this location has an ambient concentration $[CO_3^{2-}]$=106.4 mmol m^{-3}, and defines $\Delta[CO_3^{2-}] = \Delta T = \Delta C_{soft} = \Delta C_{dis} = \Delta C_{carb} = 0$. This location is again chosen because it does not have an extreme value of $[CO_3^{2-}]$ relative to the rest of the MITgcm ocean (Fig. 5a, b).

The DIC components in (5) are calculated according to the method outlined by *Williams and Follows* [2011], with full details of the carbon component decomposition for this model configuration found in *Lauderdale et al*. [2013]. To evaluate the $\frac{\partial C_{sat}}{\partial T}\Delta T$ term in (10), the same value of $\left.\frac{\partial C_{sat}}{\partial T}\right|_{A_C, P_{CO2}} \approx -0.01$ moles C m^{-3}K^{-1} [*Goodwin and Lenton*, 2009] is used along with the potential temperature field. γ is again analysed from (4) by plotting surface ocean A_T-C_{DIC} versus $[CO_3^{2-}]$ and making the assumption $\Delta[CO_3^{2-}] >> \Delta[CO_2^*]$. For the MITgcm spin-up, γ is found to be 0.70 (Fig. 6a), showing difference to the Isopycnal Box Model value of 0.64 (Fig. 4a). Relationship (10) accurately predicts $\Delta[CO_3^{2-}]$ relative to the chosen location (Fig. 6b). The prediction is accurate over most of the ocean (Fig. 5), becoming least accurate in the very deepest waters. In these locations of greatest error in the prediction, the ambient $[CO_3^{2-}]$ is low (Fig. 5a,b).

2.2.3 Synthesis

The analytical prediction (10) is in good agreement with the output of two ocean models (Figs. 3-6). The prediction shows most error in the surface ocean locations with lowest surface-ambient $[CO_3^{2-}]$ in the Isopycnal Box Model (Fig. 3), and the sub-surface ocean locations with lowest ambient $[CO_3^{2-}]$ in the MITgcm (Fig. 5). One possible reason for this is that in these locations the $[CO_2^*]$ term from (4) becomes more significant.

Values of γ are model dependent, with γ=0.64 for the Isopycnal Box Model and γ=0.7 for the MITgcm spin ups. Any model property that alters the difference between A_T and A_C may alter γ, (3) and (4), including any property that alters the difference between A_T and C_{DIC}, or the

proportion of A_T composed of A_C. What are the likely bounds for γ for the Pleistocene and Holocene oceans? To investigate this, γ is analysed for many spin-ups of the Isopycnal Box Model using different initial parameter values, varied by magnitudes broadly plausible (or greater than plausible) over glacial-interglacial cycles but not to attempt to simulate a particular past state. Four model parameters are varied to explore their impact on γ are chosen that alter global mean or spatial distributions of DIC, A_T and/or A_C: P_{CO2}; the ratio of carbon to phosphate in POC, $r_{C:P}$; global mean A_T, $\overline{A_T}$; and global mean salinity, S. Note that S alters the boric buffer contribution to A_T, and so alters the difference between A_C and A_T without altering either A_T or C_{DIC}. The steady state values of γ vary by just 0.01 as $r_{C:P}$ is varied between 100 and 120; S is varied between 33psu and 36psu; or P_{CO2} is varied between 180ppm and 280ppm. However, as $\overline{A_T}$ is increased from 2.1mol m^{-3} to 2.6mol m^{-3} γ increases from 0.60 to 0.67. The two models' preindustrial simulations show γ values of 0.64 and 0.7, and changing parameter values within one model is shown to alter γ by +/-0.04 from this initial state. Therefore, an appropriate range for γ during the Pleistocene and Holocene is likely to lie between 0.60 and 0.74, with a mid-range value of 0.67.

3 Temporal variations in global mean [CO_3^{2-}]

3.1 Theory

From (4), the global mean [CO_3^{2-}] will vary if the total amount of DIC, A_T or [CO_2^*] in the ocean varies. The global A_T budget is altered by open system $CaCO_3$ dissolution and sedimentation imbalances,

$$V\Delta\overline{A_T} = 2\Delta I_{open}, \quad (12)$$

where V is the volume of the ocean, an overbar indicates a whole-ocean average and the factor of 2 arises because each unit of dissolved $CaCO_3$ carries two units of A_T and one unit of DIC. The change in the global ocean DIC budget is given by,

$$V\Delta\overline{C_{DIC}} = \Delta I_{open} - \Delta I_{ter} - M\Delta P_{CO2}, \quad (13)$$

where M is the molar volume of the atmosphere, such that MP_{CO2} is the total amount of CO_2 in the atmosphere in moles. Subtracting (13) from (12) reveals how the global difference between A_T and DIC evolves due to perturbation,

$$V\Delta\left(\overline{A_T} - \overline{C_{DIC}}\right) = \Delta I_{open} + \Delta I_{ter} + M\Delta P_{CO2}. \quad (14)$$

Note that no knowledge of the causes of ΔP_{CO2} is required to apply (14). Taking a global average of (4), the global mean changes to [CO_3^{2-}] is written in in terms of the global mean changes to A_T, C_{DIC} and [CO_2^*],

$$\Delta\overline{[CO_3^{2-}]} = \gamma\Delta\left(\overline{A_T} - \overline{C_{DIC}}\right) + \Delta\overline{[CO_2^*]}. \quad (15)$$

Here, unlike when using (4) to consider spatial variations in [CO_3^{2-}], changes to [CO_2^*] from (15) cannot be neglected because P_{CO2} is allowed to vary in time. Substituting (15) into (14) gives a descriptive expression for the global mean change in [CO_3^{2-}],

$$V\Delta\overline{[CO_3^{2-}]} = \gamma\left(\Delta I_{open} - \Delta I_{ter} + M\Delta P_{CO2}\right) + V\Delta\overline{[CO_2^*]}. \quad (16)$$

This equation, (16), is descriptive, rather than predictive, because there is no attempt to predict the change to [CO_2^*] from either the perturbations or the initial conditions.

When surface waters are chemically saturated with respect to the overlying P_{CO2} level, [CO_2^*] is linearly related to P_{CO2}. [CO_2^*] then deviates from this linear relationship due to the C_{dis}, C_{soft}, and C_{carb} components of DIC, (5). Now consider how [CO_2^*] alters as a function of P_{CO2}, ignoring changes to C_{soft}, C_{carb} and C_{dis}. The change in global [CO_2^*] divided by the

change in P_{CO2}, $R = \dfrac{V\Delta[\overline{CO_2^*}]}{M\Delta P_{CO2}}$, is predicted from initial conditions by applying the proportionality of P_{CO2} to $[CO_2^*]$ in surface waters as an approximation over a global scale [*Goodwin and Ridgwell*, 2010], giving

$$R = \frac{V\Delta[\overline{CO_2^*}]}{M\Delta P_{CO2}} \approx \left(\frac{V[\overline{CO_2^*}]}{MP_{CO2}}\right)_{initial} . \quad (17)$$

Substituting (17) into (16) gives a predictive relationship for global mean $[CO_3^{2-}]$, valid when there is no ocean-reorganisation of DIC or A_T due to global changes to C_{soft} C_{dis} or C_{carb},

$$V\Delta[\overline{CO_3^{2-}}] = \gamma\left(\Delta I_{open} - \Delta I_{ter}\right) + M\Delta P_{CO2}\left(\gamma + R\right) . \quad (18)$$

3.2 Numerical model comparison

Starting from the initial spin-up described in Section 2.2.1 (Table 1), the Isopycnal Box Model is integrated to steady state many times with P_{CO2}, the global A_T budget and the surface phosphate restoration concentration altered independently. The model is integrated to a steady state with each combination of parameter values using: three prescribed P_{CO2} values (180, 230 and 280ppm), six global mean A_T values (2250, 2300, 2350, 2400, 2450 and 2500 mmol m^{-3}) and three prescribed surface phosphate restoration concentrations (0.25, 0.5 and 1.0mmol m^{-3}). At each of the 3x6x3=54 combinations of P_{CO2}, $\overline{A_T}$, and surface phosphate restoration concentrations, the values of $[\overline{CO_3^{2-}}]$ and $\overline{C_{DIC}}$ are recorded and ΔI_{open} and ΔI_{ter} and are calculated from mass balance arguments, (5) and (6), with $\Delta[\overline{CO_3^{2-}}] = \Delta I_{open} = \Delta I_{ter} = \Delta P_{CO2} = 0$ defined in reference to the initial spin-up (Table 1) .

Note that the model does not explicitly represent a mechanism for open system $CaCO_3$ dissolution and sedimentation, and so does not internally calculate the size of ΔI_{open}. Instead the size of ΔI_{open} is prescribed as a boundary condition, being half the change to total ocean A_T relative to the initial spin-up state, $\Delta I_{open} = V\Delta\overline{A_T}/2$, where V is total ocean volume. That ΔI_{open} is prescribed as a boundary condition, rather than internally solved by the model, does not affect the relationship between ΔI_{open} and $[CO_3^{2-}]$ being tested here.

Equation (16) is tested using prescribed perturbations to ΔI_{open}, ΔI_{ter} and ΔP_{CO2} and model output values for $\Delta[\overline{CO_2^*}]$ to calculate $\Delta[\overline{CO_3^{2-}}]$. The calculations of $\Delta[\overline{CO_3^{2-}}]$ by (16) are close to the model output $\Delta[\overline{CO_3^{2-}}]$, with the model output values consistently slightly higher than (16) (Fig. 7a). However, the aim is to use measured values of past P_{CO2} and estimates of past-ocean $[CO_3^{2-}]$ to constrain changes in $\Delta I_{open} - \Delta I_{ter}$. This descriptive relationship, (16), does not allow $\Delta I_{open} - \Delta I_{ter}$ to be constrained from reconstructed values of ΔP_{CO2} and $\Delta[\overline{CO_3^{2-}}]$, because the variable $\Delta[\overline{CO_2^*}]$ is also unconstrained. To constrain $\Delta I_{open} - \Delta I_{ter}$ from ΔP_{CO2} and $\Delta[\overline{CO_3^{2-}}]$ equation (18) must be used, since (18) removes any explicit representation of $\Delta[\overline{CO_2^*}]$.

3.2.1 Steady state comparison with constant marine biological drawdown

Consider the numerical model steady states when surface phosphate restoration concentrations are held at their initial value of 1.0mmol m^{-3} (Table 1) in each simulation, to

give identical distributions of C_{soft} and C_{carb}. Equation (18) accurately predicts $\Delta\overline{[CO_3^{2-}]}$ in terms of perturbations ΔP_{CO2}, ΔI_{ter} and ΔI_{open} when C_{soft} and C_{carb} distributions are identical between simulations (Fig. 7b, black dots and line). The difference between the $\Delta\overline{[CO_3^{2-}]}$ values predicted by (18) and simulated by model output averages 3±3mmol m^{-3}.

3.2.2 Steady state comparison with variable marine biological drawdown

Reducing the surface restored phosphate concentration in the numerical model increases $\overline{C_{soft}}$ and $\overline{C_{carb}}$ concentrations. For the smaller increase to $\overline{C_{soft}}$ and $\overline{C_{carb}}$, when surface phosphate is restored to 0.5mmol m^{-3}, (18) consistently under-predicts the steady state model value of $\Delta\overline{[CO_3^{2-}]}$ from the values of ΔP_{CO2}, ΔI_{ter} and ΔI_{open} (Fig. 7b, compare red dots to black line). The $\Delta\overline{[CO_3^{2-}]}$ values predicted by (18) average 7±1mmol m^{-3} less than the numerical model output. For the larger increase to $\overline{C_{soft}}$ and $\overline{C_{carb}}$, when surface phosphate is restored to 0.25mmol m^{-3}, (18) again consistently under-predicts the value of $\Delta\overline{[CO_3^{2-}]}$ from the values of ΔP_{CO2}, ΔI_{ter} and ΔI_{open} (Fig. 7b, compare blue dots to black line). This time the $\Delta\overline{[CO_3^{2-}]}$ values predicted by (18) average 10±1mmol m^{-3} less than the model output.

3.3.3 Numerical model comparison over a range of timescales

This section compares (18) to a numerical model simulation spanning 12000 model years to consider the timescales over which (18) is valid. The Isopycnal Box Model does not contain interactive representation of terrestrial carbon storage or $CaCO_3$ sediments. Therefore, to test the timescales over which the theory is valid, (18) is compared to numerical model output of the Isopycnal Box Model in which prescribed temporal variations in ΔI_{ter} and ΔI_{open} (Fig. 8a) are applied to an initial steady state spin-up (Table 1). The terrestrial carbon reservoir is increased by 500PgC over 500 years (Fig. 8a), removing 500PgC carbon from the atmosphere-ocean system. In addition, a prescribed $CaCO_3$ precipitation removes 450PgC during carbonate compensation over 10 000 years (Fig. 8a), removing A_T and DIC in a 2:1 ratio from the bottom two layers of the sub-surface ocean.

Initially, P_{CO2} falls in response to the terrestrial carbon uptake (Fig. 8), while $\overline{[CO_3^{2-}]}$ simultaneously increases as DIC is outgassed from the ocean due to the lower P_{CO2}. During this initial period, the theory incorrectly predicts a fall in $\overline{[CO_3^{2-}]}$ (Fig. 8c), because (18) assumes that the ocean is always in chemical equilibrium with the atmosphere. Around 1000 years after the terrestrial carbon reservoir begins to change (18) becomes more accurate as the rate of change in P_{CO2} slows (Fig. 8c). The agreement between the theory and numerical model output on timescales longer than ocean overturning (Fig. 8) shows that (18) is valid between 1000 and 10 000 year timescales when carbonate compensation processes are ongoing, but is not valid when significant air-sea CO_2 exchange occurs on timescales shorter than ocean overturning.

4 Temporal variations to local $[CO_3^{2-}]$

4.1 Theory

The change over time of $[CO_3^{2-}]$ at one location is written in terms of the change over time of the global mean, plus the change over time of the difference between local $[CO_3^{2-}]$ and global mean $[CO_3^{2-}]$,

$$\Delta[CO_3^{2-}] = \Delta\overline{[CO_3^{2-}]} + \Delta\left([CO_3^{2-}] - \overline{[CO_3^{2-}]}\right). \quad (19)$$

The difference, at any one time, between local $[CO_3^{2-}]$ and global mean $[CO_3^{2-}]$ is calculated by imagining the global mean $[CO_3^{2-}]$ as the concentration at one specific spatial location. Thus, (10) gives

$$[CO_3^{2-}] - \overline{[CO_3^{2-}]} \approx \gamma\left(-\left.\frac{\partial C_{sat}}{\partial T}\right|_{A_C, P_{CO2}}\left(T-\overline{T}\right) - \left(C_{soft} - \overline{C_{soft}}\right) - \left(C_{dis} - \overline{C_{dis}}\right) + \left(C_{carb} - \overline{C_{carb}}\right)\right). \quad (20)$$

Combining (19) with (20) and (18) gives an approximate relationship for the change in local $[CO_3^{2-}]$ over time,

$$\Delta[CO_3^{2-}] \approx \left(\frac{\gamma\left(\Delta I_{open} - \Delta I_{ter}\right) + M\Delta P_{CO2}\left(\gamma + R\right)}{V}\right) + \gamma\left(-\left.\frac{\partial C_{sat}}{\partial T}\right|_{A_C, P_{CO2}}\Delta\left(T-\overline{T}\right) - \Delta\left(C_{soft} - \overline{C_{soft}}\right) - \Delta\left(C_{dis} - \overline{C_{dis}}\right) + \Delta\left(C_{carb} - \overline{C_{carb}}\right)\right). \quad (21)$$

This approximation assumes that the change over time in the difference between the local and global mean $[CO_3^{2-}]$ is equivalent to the change in the difference between two locations in space. This derivation of (21) assumes the value of γ does not alter if P_{CO2} alters, and that ocean reorganisations of DIC and A_T have no impact on global mean $[CO_2^*]$.

4.2 Numerical Model comparison

The prediction for the local change to $[CO_3^{2-}]$ between two different time periods (21) is tested using two steady states of the Isopycnal Box Model. The initial spin-up (Table 1) is compared to the steady state with $\overline{A_T}$ =2500 mmol m^{-3}, P_{CO2} = 180 ppm and surface restored phosphate of 0.25 mmol m^{-3}. The reduction to surface restored phosphate increases global mean C_{soft} and C_{carb}. The model difference in $[CO_3^{2-}]$ for each box is analysed between these two states, and compared to the analytical prediction (Fig. 9).

The changes in local $[CO_3^{2-}]$ between the two model states show considerable variation, from changes of circa -5 mmol m^{-3} to circa +80 mmol m^{-3} (Fig. 9). This high spread in the local change to $[CO_3^{2-}]$ is due to the changes in C_{soft} and C_{carb} between the two states. The predicted changes to local $[CO_3^{2-}]$ from (21) are reasonably accurate (Fig. 9), but the accumulation of small errors from many approximations leads to increased model-theory discrepancy. For the majority of ocean boxes, the predicted local $\Delta[CO_3^{2-}]$ is more positive than the modelled change (Fig. 9), due to the systematic offset introduced by assuming in (21) that changing C_{soft} and C_{carb} has no impact on the accuracy of (18) (Fig. 7b).

5. Implications for the causes of Glacial-Interglacial CO_2 change

Yu et al [2010] reconstruct $[CO_3^{2-}]$ at five locations for the Last Glacial Maximum (LGM), Deglacial Peak and late Holocene from foraminifer B/Ca ratios. The changing spatial patterns of these $[CO_3^{2-}]$ reconstructions are now analysed using the quantitative theory (10). The global mean changes in $[CO_3^{2-}]$ between LGM, Deglacial Peak and late Holocene are not analysed using the quantitative theory (18) because accurate use of (18) requires the global mean C_{soft} and C_{carb} to be the same at the LGM as the late Holocene (see Fig. 7b), and this cannot be assumed.

Rearranging (10) relates the spatial gradient in carbon stored through different processes to the spatial gradient in $[CO_3^{2-}]$,

$$\frac{\partial C_{sat}}{\partial T}\Delta T + \Delta C_{soft} + \Delta C_{dis} - \Delta C_{carb} = -\frac{\Delta[CO_3^{2-}]}{\gamma}. \quad (22)$$

Applying (22) to the reconstructed [CO_3^{2-}] of *Yu et al* [2010] now reveals the spatial differences in $\left(\partial C_{sat}/\partial T\right)T + C_{soft} + C_{dis} - C_{carb}$ during the Late Holocene, Deglacial Peak and LGM between the five locations. Table 2 shows the how $\left(\partial C_{sat}/\partial T\right)T + C_{soft} + C_{dis} - C_{carb}$ varies spatially relative to the intermediate North Atlantic, NA, location during each period. The Intermediate NA is chosen as the reference because it is likely to have contained newly ventilated water across each time period, with evidence suggesting a shoaled but significant Atlantic Meridional Overturning Circulation at the LGM [*Lippold et al*, 2012]. C_{soft} and C_{carb} are initially zero in newly-subducted water. Continual regeneration of falling POC in the ocean interior causes C_{soft} and C_{carb} concentrations to increase with water-age [*Sarmiento and Gruber*, 2006]. Ocean locations that retain newly ventilated water across different time periods are thus likely to have the smallest and most stable concentrations of C_{soft} and C_{carb}, and thus be good reference locations for (22), because the water age varies least between time periods. During all three time-periods, the Intermediate NA has the lowest value of $\left(\partial C_{sat}/\partial T\right)T + C_{soft} + C_{dis} - C_{carb}$ (Table 2), consistent with it retaining newly ventilated water that has not had time for significant C_{soft} build-up.

Relative to the Intermediate NA, the concentrations of $\left(\partial C_{sat}/\partial T\right)T + C_{soft} + C_{dis} - C_{carb}$ in the rest of the ocean are elevated considerably more in the LGM than the late Holocene (Table 2), with implications for the causes of the glacial-interglacial change in P_{CO2}. Combining the relationship for P_{CO2} on millennial timescales in terms of C_{soft}, C_{dis} and C_{carb} [equation (24) in *Goodwin et al*, 2008] with the relationship in terms of $\left(\partial C_{sat}/\partial T\right)T$ [equation A4 in *Goodwin et al*, 2011] gives,

$$P_{CO2}(\text{final}) = P_{CO2}(\text{initial})\exp\left(\frac{V\left(\Delta\overline{C_{soft}} + \Delta\overline{C_{dis}} + \left(\partial C_{sat}/\partial T\right)\Delta\overline{T}\right)}{I_B}\right).$$
$$\left(\frac{I_{O(A-C)}}{I_{O(A-C)} - V\Delta\overline{C_{carb}}}\right)\exp\left(\frac{MP_0V\Delta\overline{C_{carb}}}{\left(I_{O(A-C\}} - V\Delta\overline{C_{carb}}\right)I_B}\right), \quad (23)$$

where I_B is the buffered carbon inventory and $I_{O(A\text{-}C)}$ is the whole ocean difference between A_T and C_{DIC} [see *Goodwin et al*, 2008 for parameter values]. Therefore, to estimate the impact on P_{CO2}, the global mean changes to C_{soft}, C_{carb}, C_{dis} and T must be estimated.

Scaling the concentration changes (Table 2) with approximate volumes for each region reveals that during the LGM, global $\left(\partial C_{sat}/\partial T\right)T + C_{soft} + C_{dis} - C_{carb}$ increased in the rest of the global ocean relative to the Intermediate NA (Table 2) by circa 770±200PgC. This assumes that: (1) the Pacific basin represents half the total ocean volume, and the Indian and Atlantic basins each represent a quarter, and (2) the Intermediate ocean (being the upper ~2000m) represents 2/5 of total ocean volume while the deep ocean (being ~2000m to ~5000m depth) represents 3/5.

The impact this estimated 570 to 970PgC increase, relative to the Intermediate NA, had on P_{CO2} depends crucially on the LGM to Holocene change to $\left(\partial C_{sat}/\partial T\right)T + C_{soft} + C_{dis} - C_{carb}$ within the Intermediate NA. If Intermediate NA $\left(\partial C_{sat}/\partial T\right)T + C_{soft} + C_{dis} - C_{carb}$ was the same in the LGM as the Holocene, the increase in in the rest of the ocean is enough to decrease

P_{CO2} by 40 to 70ppm during the LGM (23). Thus, under this assumption, circa 40 to 70% of the observed glacial decrease in P_{CO2} is explained by the combined effects of four terms: increases in C_{soft} and C_{dis} and/or decreases in T and C_{carb}.

However, if Intermediate NA $\left(\partial C_{sat}/\partial T\right)T + C_{soft} + C_{dis} - C_{carb}$ was increased at the LGM then the estimated range, 570 to 590PgC, would be an underestimate, and if Intermediate NA $\left(\partial C_{sat}/\partial T\right)T + C_{soft} + C_{dis} - C_{carb}$ was decreased then the estimated range is an overestimate. The $(\partial C_{sat}/\partial T)T$ term is likely to have increased during the LGM relative to the late Holocene, because $\left(\partial C_{sat}/\partial T\right)$ is negative and temperatures in the NA were cooled during the LGM [*Waelbroeck et al*, 2009]. There are currently no proxy-based reconstructions of C_{soft}, C_{dis}, C_{carb} during the LGM to test how these terms altered. However, evidence that the Intermediate NA remained newly ventilated [*Lippold et al*, 2012] provides confidence that C_{soft} and C_{carb} both remained small there at the LGM, while the magnitude of C_{dis} is generally small in comparison to C_{soft} or C_{carb} [*Ito and Follows*, 2005; *Williams and Follows*, 2011].

6. Discussion

In this study the relationships between $[CO_3^{2-}]$ and ocean carbon cycle processes are identified for both spatial, (10), and temporal, (16), (18) and (21), variations. These quantitative relationships are in good agreement with the output of numerical models (Figs. 3-9), allowing additional quantitative information to be gained from spatial and temporal $[CO_3^{2-}]$ paleo-reconstructions. This quantitative information is expressed in terms of a process driven view of ocean carbon storage [*Ito and Follows*, 2005; *Williams and Follows*, 2011], and so can be used to provide additional constraints on the causes of P_{CO2} change.

The spatial variation in $[CO_3^{2-}]$ between two sites at the same time is accurately related to the differences in carbon storage from, (10), remineralised soft tissue, ΔC_{soft}, disequilibrium carbon, ΔC_{dis}, temperature-solubility, $(\partial C_{sat}/\partial T)\Delta T$, and remineralised marine $CaCO_3$, ΔC_{carb}, by (Figs 3-6). Thus, reconstructing local $[CO_3^{2-}]$ for the same time period at two sites is an effective method of comparing the combined difference in local carbon storage and temperature-solubility between those two sites (Table 2). Additional proxies will be required to separate the contributions of the individual terms.

Temporal changes to the global mean $[CO_3^{2-}]$ are accurately predicted from the change in atmospheric CO_2, ΔP_{CO2}, the open system $CaCO_3$ dissolution, ΔI_{open}, and the change in carbon stored by the terrestrial biosphere, ΔI_{ter}, (18), only when global C_{soft} and C_{carb} concentrations are held constant (Fig. 7b). Future work will examine how the global-mean $[CO_3^{2-}]$ theory (18) can be modified to accommodate variations to C_{soft} and C_{carb}. A change to local $[CO_3^{2-}]$ over time can be the result of 7 different terms, (21) (Fig. 9): ΔI_{open}, ΔI_{ter}, ΔP_{CO2}, $\Delta\left(T - \overline{T}\right)$, $\Delta\left(C_{soft} - \overline{C_{soft}}\right)$, $\Delta\left(C_{dis} - \overline{C_{dis}}\right)$ and $\Delta\left(C_{carb} - \overline{C_{carb}}\right)$.

Acknowledgements

This research was funded by UK NERC postdoctoral fellowship NE/I020725/1 and the Herchel Smith Postdoctoral Fellowship Fund. JML acknowledges funding from a UK NERC PhD Studentship (NER/S/A/2006/14210) and grant NE/G018782/1. Constructive points from two anonymous reviewers greatly improved the quality of the manuscript.

References

Archer, D. (1991), Modeling the calcite lysocline, *J. Geophys. Res.*, *96*(C9), 17,037–17,050, doi:10.1029/91JC01812.

Broecker, W. S (1982a), Glacial to interglacial changes in ocean chemistry, *Prog. Oceanogr., 11,* 151- 197.

Broecker, Wallace S. (1982b), Ocean Chemistry During Glacial Time, *Geochimica et Cosmochimica Acta,* 46, 1689-1705.

Chiu, T.-C., and W. S. Broecker (2008), Toward better paleocarbonate ion reconstructions: New insights regarding the CaCO3 size index, *Paleoceanography*, 23, PA2216, doi:10.1029/2008PA001599.

Dutkiewicz, S., M. J. Follows, and P. Parekh (2005), Interactions of the iron and phosphorus cycles: A three dimensional model study, *Global Biogeochem. Cycles*, 19, GB1021, doi: 10.1029/2004GB002342.

Elderfield, H., J. Yu, P. Anand, T. Keifer and B. Nyland (2006), Calibrations for benthic foraminiferal Mg/Ca paleothermometry and the carbonate ion hypothesis, *Earth and Planet. Sci. Lett.*, 250, 3-4, 633-649, doi:10.1016/j.epsl.2006.07.041.

Fofonoff, N. P. (1985), Physical properties of seawater: A new salinity scale and equation of state for seawater, *J. Geophys. Res.,*90, 3322–3342. doi:10.1029/JC090iC02p03332.

Follows, M. J., S. Dutkiewicz, and T. Ito (2006), On the solution of the carbonate system in ocean biogeochemistry models, *Ocean Modell.*, 12, 290 – 301. doi:10.1016/j.ocemod.2005.05.004

Goodwin, P. (2012), An Isopycnal Box Model with predictive deep-ocean structure for biogeochemical cycling applications, *Ocean Modell.*, doi:10.1016/j.ocemod.2012.04.005.

Goodwin, P., K. I. C. Oliver, and T. M. Lenton (2011), Observational constraints on the causes of Holocene CO2 change, *Global Biogeochem. Cycles*, 25, GB3011, doi:10.1029/2010GB003888.

Goodwin, P., and A. Ridgwell (2010), Ocean-atmosphere partitioning of anthropogenic carbon dioxide on multimillennial timescales, *Global Biogeochem. Cycles*, 24, GB2014, doi:10.1029/2008GB003449.

Goodwin, P., and T. M. Lenton (2009), Quantifying the feedback between ocean heating and CO2 solubility as an equivalent carbon emission, *Geophys. Res. Lett*., 36, L15609, doi:10.1029/2009GL039247.

Goodwin, P., M. J. Follows, and R. G. Williams, (2008), Analytical relationships between atmospheric carbon dioxide, carbon emissions, and ocean processes, *Global Biogeochem. Cycles*, *22*, GB3030, doi:10.1029/2008GB003184.

Gruber, N., J. L. Sarmiento, and T. F. Stocker (1996), An improved method for detecting anthropogenic CO_2 in the oceans, *Global Biogeochem. Cycles*, 10, 809-837.

584 Hodell, D.A., Charles, C.D., and Sierro, F.J. (2001), Late Pleistocene evolution of the ocean's
585 carbonate system, *Earth Planetary Science Letters*, 192, 109-124.
586
587 Ito, T., and M. J. Follows, (2005), Preformed phosphate, soft tissue pump and atmospheric
588 CO2, *J. Mar. Res.*, 63(4), 813– 839, doi:10.1357/0022240054663231.
589
590 Jiang, S., P. Stone, and P. Malanotte-Rizzoli (1999) An assessment of the Geophysical Fluid
591 Dynamics Laboratory ocean model with coarse resolution: Annual-mean climatology, *J.*
592 *Geophys. Res.*, 104, 25623–25645.
593
594 Lauderdale, J.M., Naveira Garabato, A.C., Oliver, K.I.C., Follows, M.J. and Williams, R.G.
595 (2013) Wind-driven changes in Southern Ocean residual circulation, ocean carbon reservoirs
596 and atmospheric CO2, *Climate Dynamics*, doi:10.1007/s00382-012-1650-3
597
598 Lippold, J., Y. Luo, R. Francois, S. E. Allen, J. Gherardi, S. Pichat, B. Hickey, H. Schulz
599 (2012) Strenth and Geometry of the glacial Atlantic Meridional Overturning Circulation,
600 *Nature Geoscience*, 5, p813-816, doi:10.1038/ngeo1608.
601
602 Marchitto, T. M., J. Lynch-Stieglitz, and S. R. Hemming (2005), Deep Pacific $CaCO_3$
603 compensation and glacial-interglacial atmospheric CO_2, *Earth Planet. Sci. Lett.*, *231*, 317–
604 336, doi:10.1016/j.epsl.2004.12.024.
605
606 Marinov, I., M. Follows, A. Gnanadesikan, J. L. Sarmiento, and R. D. Slater (2008), How
607 does ocean biology affect atmospheric *p*CO2? Theory and models, *J. Geophys. Res.*, *113*,
608 C07032, doi:10.1029/2007JC004598.
609
610 Marshall, J., A. Adcroft, C. Hill, L. Perelman, and C. Heisey (1997) A finite-volume,
611 incompressible Navier Stokes model for studies of the ocean on parallel computers, J.
612 Geophys. Res., 102(C3), 5753– 5766.
613
614 Martin, J. H., G. A. Knauer, D. M. Karl, and W. W. Broenkow (1987), VERTEX: carbon
615 cycling in the northeast Pacific, *Deep-Sea Research*, 34, 2, 267-285.
616
617 Omta, A. W., S. Dutkiewicz, and M. J. Follows (2011), Dependence of the ocean-atmosphere
618 partitioning of carbon on temperature and alkalinity, *Global Biogeochem. Cycles*, 25,
619 GB1003, doi:10.1029/2010GB003839.
620
621 Parekh, P., M. J. Follows, and E. Boyle (2005), Decoupling of iron and phosphate in the
622 global ocean, *Global Biogeochem. Cycles*, 19, GB2020, doi:10.1029/2004GB002280.
623
624 Ridgwell, A. and R.E. Zeebe (2005) The role of the global carbonate cycle in the regulation
625 and evolution of the Earth system, *Earth and Planetary Science Letters*, 234, 299–315.
626 doi:10.1016/j.epsl.2005.03.006.
627
628 Sarmineto, J. L. and N. Gruber (2006), *Ocean Biogeochemical Dynamics*, 503pp., Princeton
629 University Press.
630
631 Sigman, D. M. and E. A. Boyle (2000), Glacial/Interglacial variations in atmospheric carbon
632 dioxide, *Nature*, 407, 859-869, doi:10.1038/35038000.
633

634 Sigman, D. M., D. C. McCorkle, and W. R. Martin (1998), The calcite lysocline as a
635 constraint on glacial/interglacial low-latitude production changes, *Global Biogeochem.*
636 *Cycles*, *12*(3), 409–427, doi:10.1029/98GB01184.
637
638 Trenberth, K., J. Olson, and W. Large (1989), A global wind stress climatology based on
639 ECMWF analyses, Tech. rep., NCAR/TN- 338+STR, National Centre for Atmospheric
640 Research, Boulder, Colorado.
641
642 Yu, J., W. S. Broecker, H. Elderfield, Z. Jin, J. McManus and F. Zhang (2010), Loss of
643 Carbon from the Deep Sea Since the Last Glacial Maximum, *Science*, 330, 1084-1087,
644 doi:10.1126/science.1193221.
645
646 Yu, J., and H. Elderfield (2007), Benthic foraminiferal B/Ca ratios reflect deep water
647 carbonate saturation state, *Earth Planet. Sci. Lett.*, 258, 73–86,
648 doi:10.1016/j.epsl.2007.03.025.
649
650 Waelbroeck, C. et al (2009), Constraints on the magnitude and patterns of ocean cooling at
651 the Last Glacial Maximum, *Nature Geoscience*, 2, 127-132, doi:10.1038/ngeo411.
652
653 Williams, R. G., and M. J. Follows (2011), *Ocean dynamics and the carbon cycle: principals*
654 *and mechanisms*, 416 pp., Cambridge University Press.
655

Tables

Isopycnal Box Model parameter	Value
Exponential decay length scale of particulate $CaCO_3$ dissolution below euphotic zone	3500m
Particulate Organic Carbon (POC) remineralisation power law exponent, b (11), after *Martin et al* [1987]	1.0
Depth of Euphotic Zone for POC and Particulate $CaCO_3$ remineralisation, z_c	75m
Global mean titration alkalinity concentration, $\overline{A_T}$	2350 mmol m^{-3}
Fixed atmospheric CO_2 level, P_{CO2}	280ppm
Air-sea CO_2 gas transfer coefficient, k_g	5×10^{-5} m s^{-1}
Global mean phosphate concentration	2.2 mmol m^{-3}
Surface phosphate restoring concentration	1.0 mmol m^{-3}
Ratio of Carbon to Phosphate in POC	105 moles Carbon per mole Phosphate
Ratio of $CaCO_3$ to POC exiting euphotic zone	0.1 moles $CaCO_3$ per mole POC

Table 1: Biogeochemical parameters used in the initial spin up of the Isopycnal Box Model. Other model parameters are as for the tuned idealised preindustrial set-up described in *Goodwin* [2012].

	Deep North Atlantic (μmol C kg^{-1})	West Equatorial Pacific (μmol C kg^{-1})	Intermediate Equatorial Pacific (μmol C kg^{-1})	Abyssal Indo-Pacific (μmol C kg^{-1})
Late Holocene	9±9	49±7	61±8	41±6
Deglacial Peak	18±6	55±7	71±9	31±6
LGM	86±6	107±12	108±12	83±10

Table 2: The spatial differences in $C_{soft} + C_{dis} + (\partial C_{sat}/\partial T)T - C_{carb}$ relative to the Intermediate North Atlantic in the Late Holocene, Deglacial Peak and LGM. Values are calculated from (22) using the reconstructed carbonate ion concentrations of *Yu et al* [2010]. A γ value of 0.67±0.07 is assumed, consistent with γ lying in the range 0.60 to 0.74.

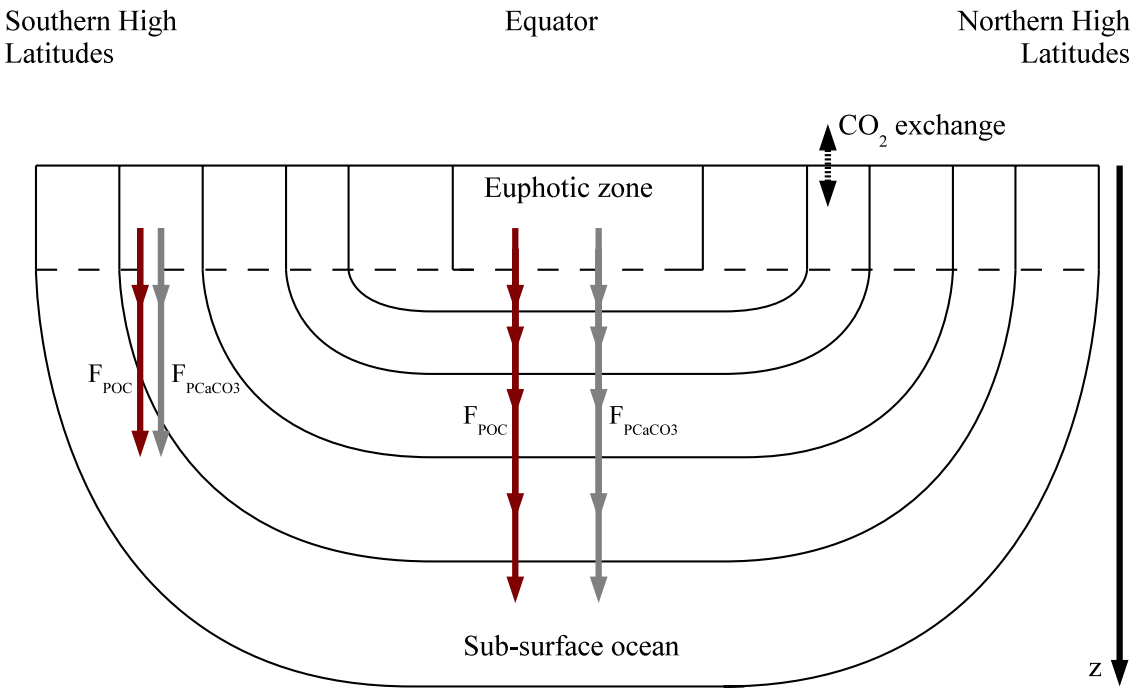

669
670
671 Figure 1: Schematic of the Isopycnal Box Model with coupled carbon cycle. CO_2 exchange
672 occurs across the air-sea interface (black dashed arrow). Fluxes of particulate organic carbon
673 (F_{POC} - red arrows) and particulate $CaCO_3$ (F_{PCaCO3} – grey arrows) leave the boxes in the
674 euphotic zone and reineralise at depth. When calculating the remineralisation profile, the
675 depth of each sub-surface box varies with latitude, illustrated by comparing the two
676 illustrated sites of F_{CaCO3} and F_{POC}.
677

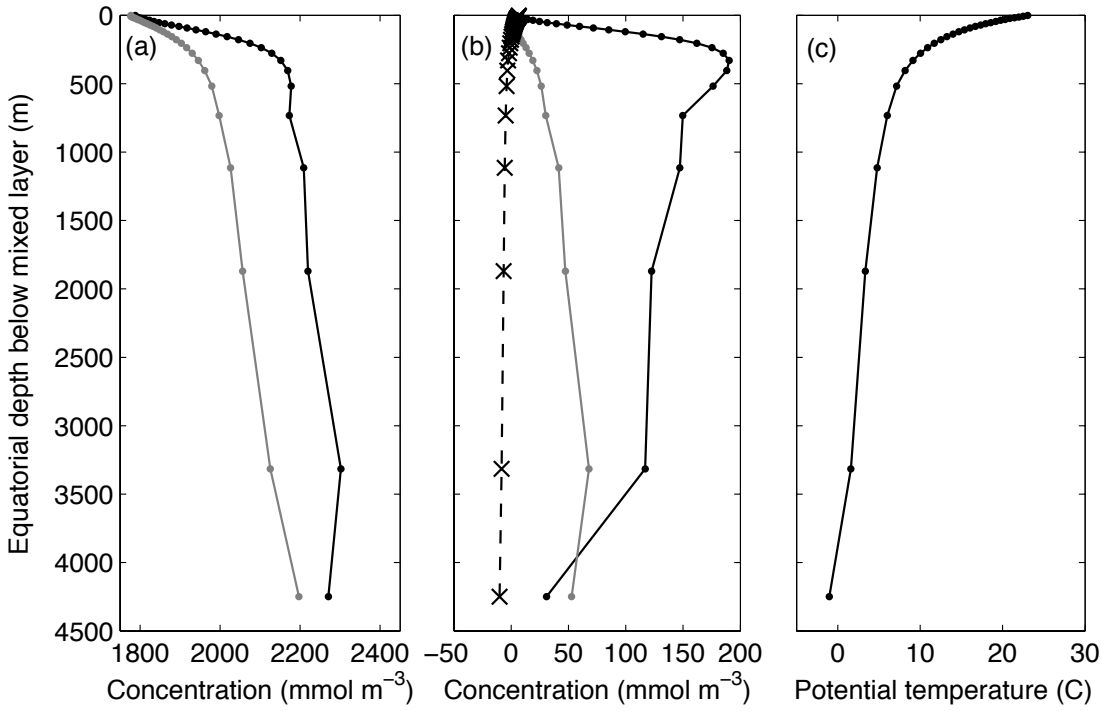

Figure 2: The DIC components and potential temperature in the initial Isopycnal Box Model spin-up versus depth below the mixed layer at the equator. (a) C_{DIC} (black dots and line) and C_{sat} (grey dots and line). (b) C_{soft} (black dots and line), C_{carb} (grey dots and line) and C_{dis} (black crosses and dashed line). (c) Potential temperature (black dots and line).

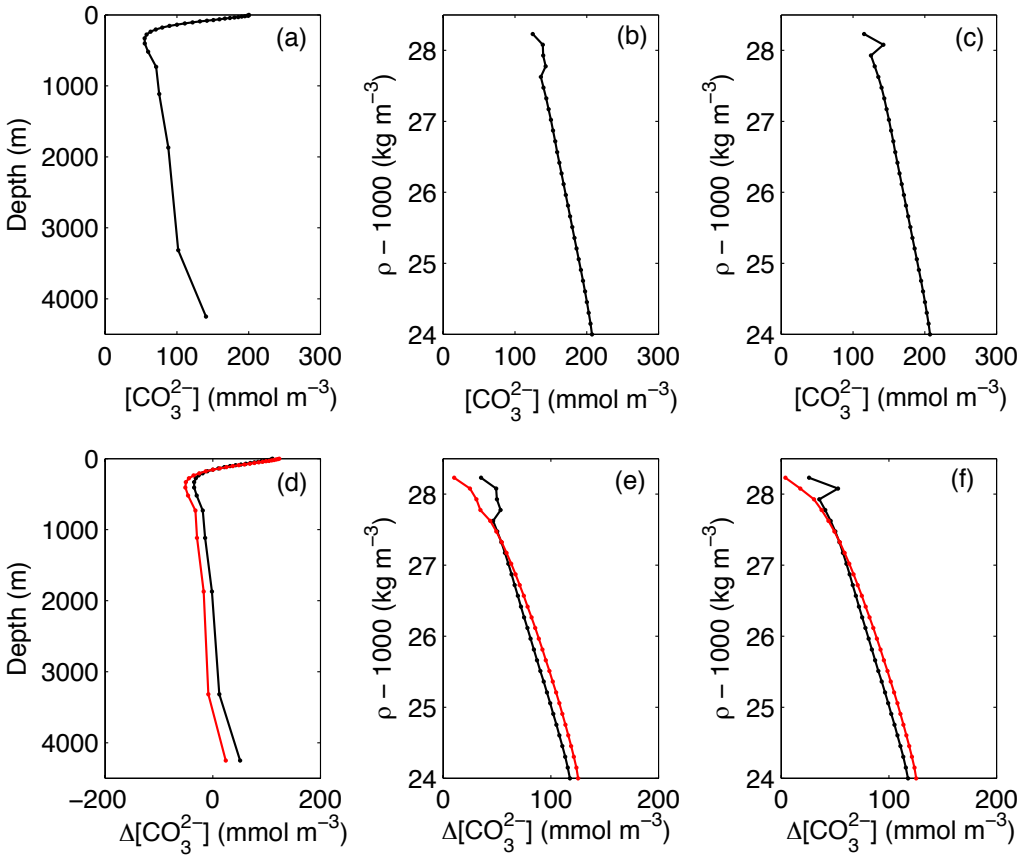

Figure 3: Ambient $[CO_3^{2-}]$ and spatial $[CO_3^{2-}]$ anomaly relative to a chosen box in the Isopycnal Box Model spin-up. (a) $[CO_3^{2-}]$ versus depth below the mixed layer at the equator in the sub-surface boxes. (b) $[CO_3^{2-}]$ versus potential density in the southern hemisphere surface boxes. (c) $[CO_3^{2-}]$ versus potential density in the northern hemisphere surface boxes. Spatial $[CO_3^{2-}]$ anomalies in the numerical model output (black) and theoretical prediction, (10), (red) are shown versus depth in the sub surface ocean (d), and versus density in the southern and northern hemisphere surface boxes, (e) and (f) respectively. Spatial $[CO_3^{2-}]$ anomaly is referenced with respect to the ρ=1026.4kg m^{-3} sub-surface box, which lies 156m deep below the mixed layer at the equator.

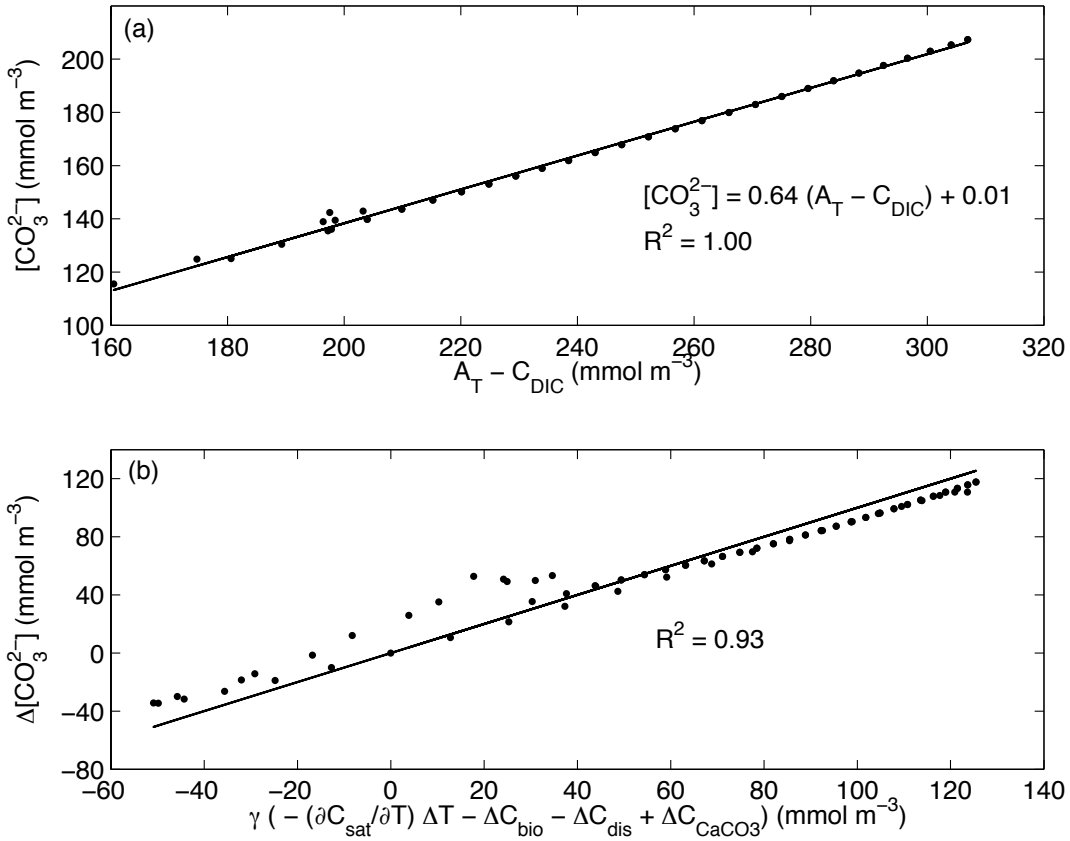

Figure 4: Spatial variations in $[CO_3^{2-}]$ in the Isopycnal Box Model and theoretical prediction (10). (a) $[CO_3^{2-}]$ against A_T-C_{DIC} in the surface ocean boxes of the Isopycnal Box Model (dots). The line of best fit (solid line) reveals a value of γ=0.64, (4). (b) $\Delta[CO_3^{2-}]$ against $\gamma\left(-\frac{\partial C_{sat}}{\partial T}\Delta T - \Delta C_{bio} - \Delta C_{dis} + \Delta C_{CaCO3}\right)$ in surface and sub-surface boxes of the Isopycnal Box Model (dots) against the theoretical prediction (10) (solid line). The spatial changes are referenced by setting $\Delta[CO_3^{2-}] = \Delta T = \Delta C_{soft} = \Delta C_{dis} = \Delta C_{carb} = 0$ in the ρ=1026.4kg m^{-3} sub-surface box

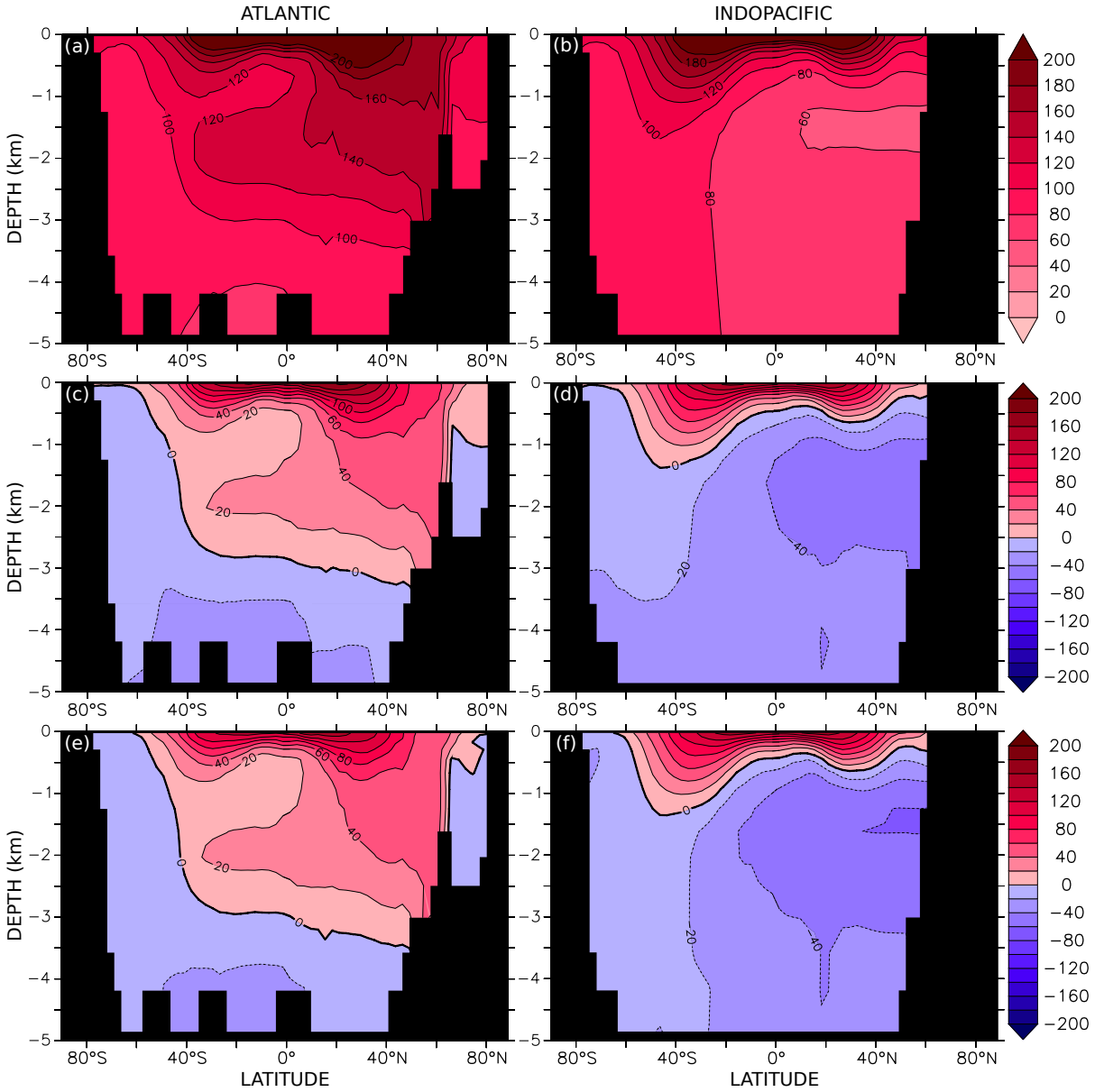

Figure 5: MITgcm carbonate ion concentrations and spatial anomalies. Annual average $[CO_3^{2-}]$ in (a) Atlantic and (b) Indopacific basins. Annual average $\Delta[CO_3^{2-}]$ in (c) Atlantic and (d) Indopacific basins. Annual average $\gamma\left(-\frac{\partial C_{sat}}{\partial T}\Delta T - \Delta C_{soft} - \Delta C_{dis} + \Delta C_{CaCO3}\right)$ in (e) the Atlantic and (f) the Indopacific basins. To calculate the spatial anomalies, $\Delta[CO_3^{2-}] = \Delta T = \Delta C_{soft} = \Delta C_{dis} = \Delta C_{carb} = 0$ is defined at 142°W, 43.5°S and 1250 m depth and γ=0.7 is used.

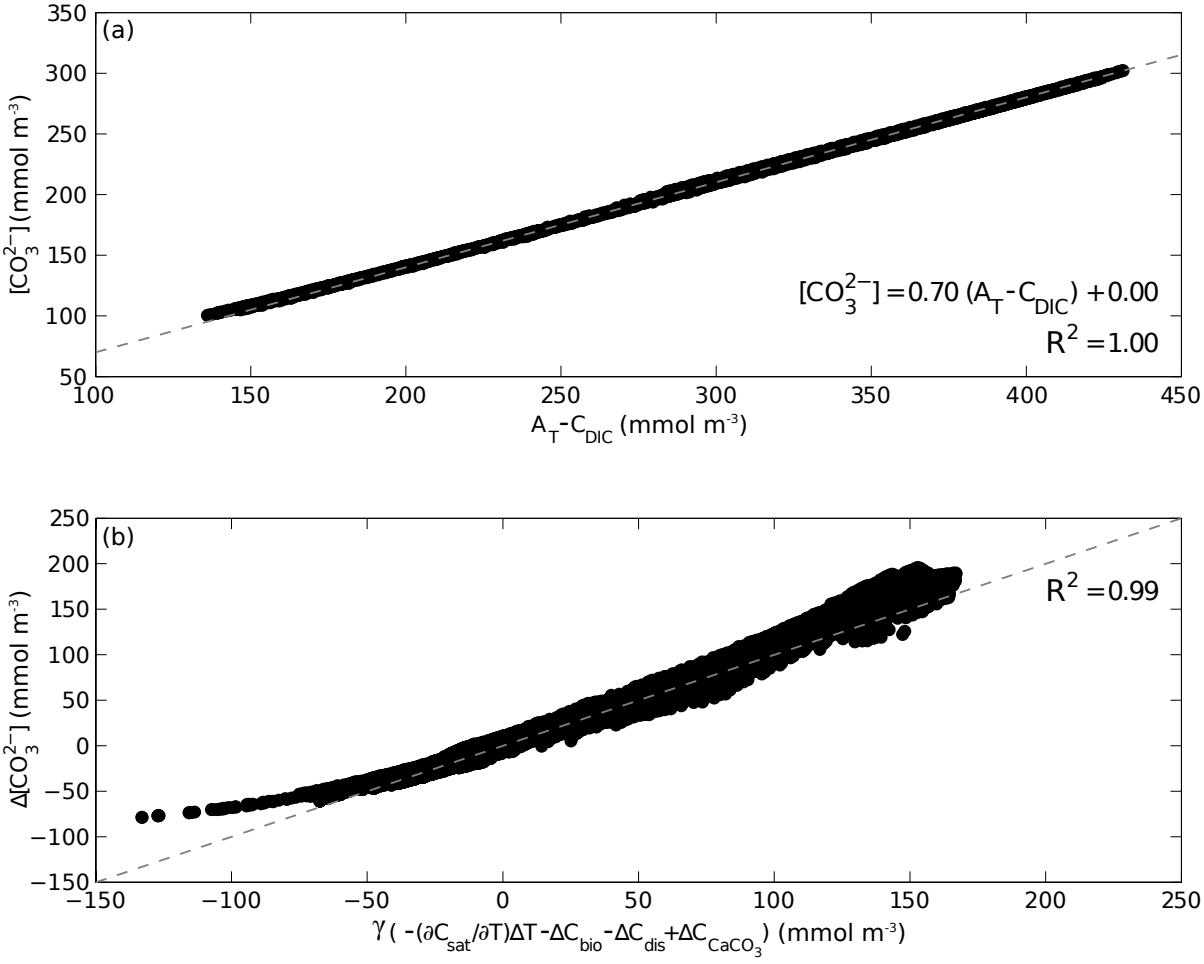

Figure 6: Spatial variations in $[CO_3^{2-}]$ in the MITgcm and theoretical prediction (10). (a) $[CO_3^{2-}]$ against A_T-C_{DIC} in the surface ocean of the MITgcm (dots). The line of best fit (dotted line) reveals a value of γ=0.70, (4). (b) $\Delta[CO_3^{2-}]$ against $\gamma\left(-\frac{\partial C_{sat}}{\partial T}\Delta T - \Delta C_{bio} - \Delta C_{dis} + \Delta C_{CaCO3}\right)$ at all ocean locations in the MITgcm (dots) against the theoretical prediction (10) (dotted line). The spatial changes are referenced by setting $\Delta[CO_3^{2-}] = \Delta T = \Delta C_{soft} = \Delta C_{dis} = \Delta C_{carb} = 0$ below the pycnocline in the Pacific sector of the Southern Ocean at 142°W, 43.5°S and 1250 m depth.

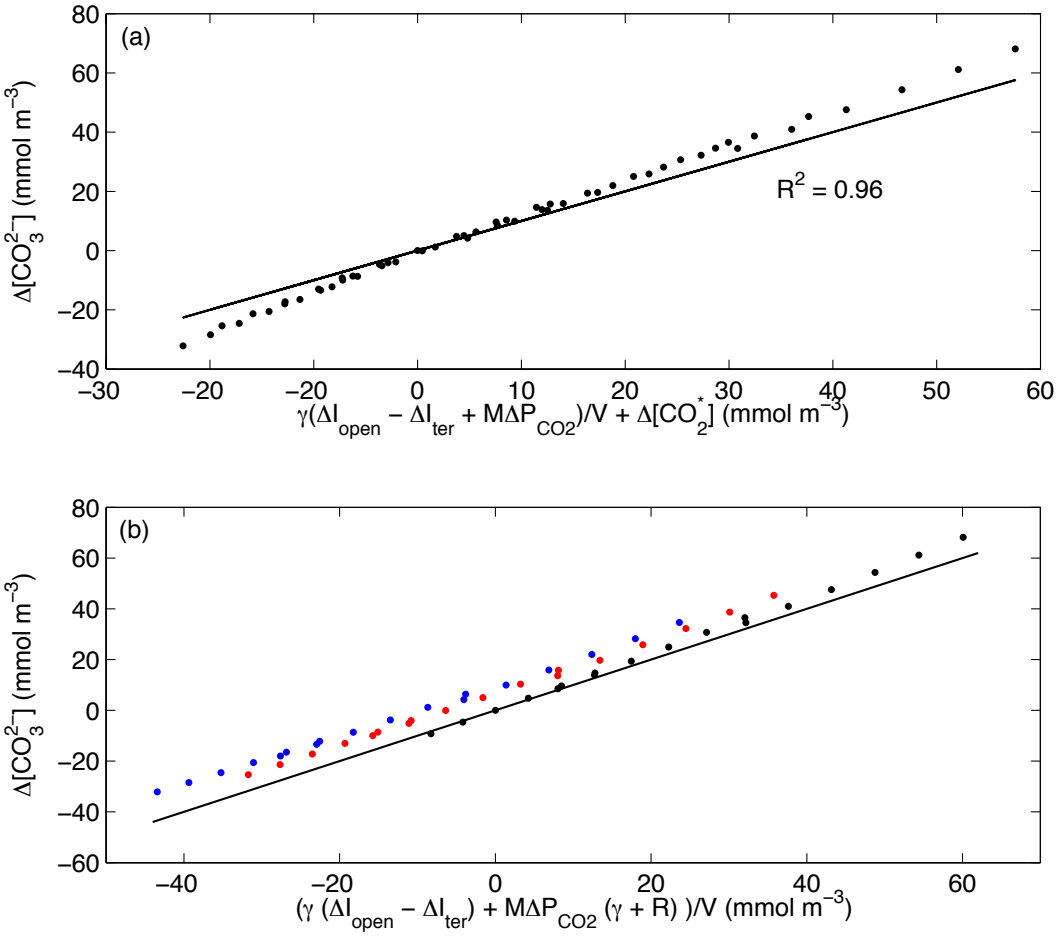

Figure 7: Variations in global mean $[CO_3^{2-}]$ in the Isopycnal Box Model predicted using (a) equation (16) and (b) equation (18), with γ analysed from Figure 3a. (a) Isopycnal Box Model output when the system reaches steady state (dots) and theoretical analysis from (14) (line), where $[CO_3^{2-}]$ in the theoretical analysis is taken from model output. (b) Isopycnal box model output (dots) and the theoretical prediction (line) using (18) and assuming a constant R (17). The Isopycnal Box Model output has scenarios that have surface phosphate restoration concentrations unaltered at 1 mmol m^{-3} (black dots), reduced by half to 0.5 mmol m^{-3} (red dots), and reduced by half-again to 0.25 mmol m^{-3} (blue dots). The vertical offset between red and blue dots relative to the solid line indicates that changes to biological carbon drawdown affects the accuracy of (18).

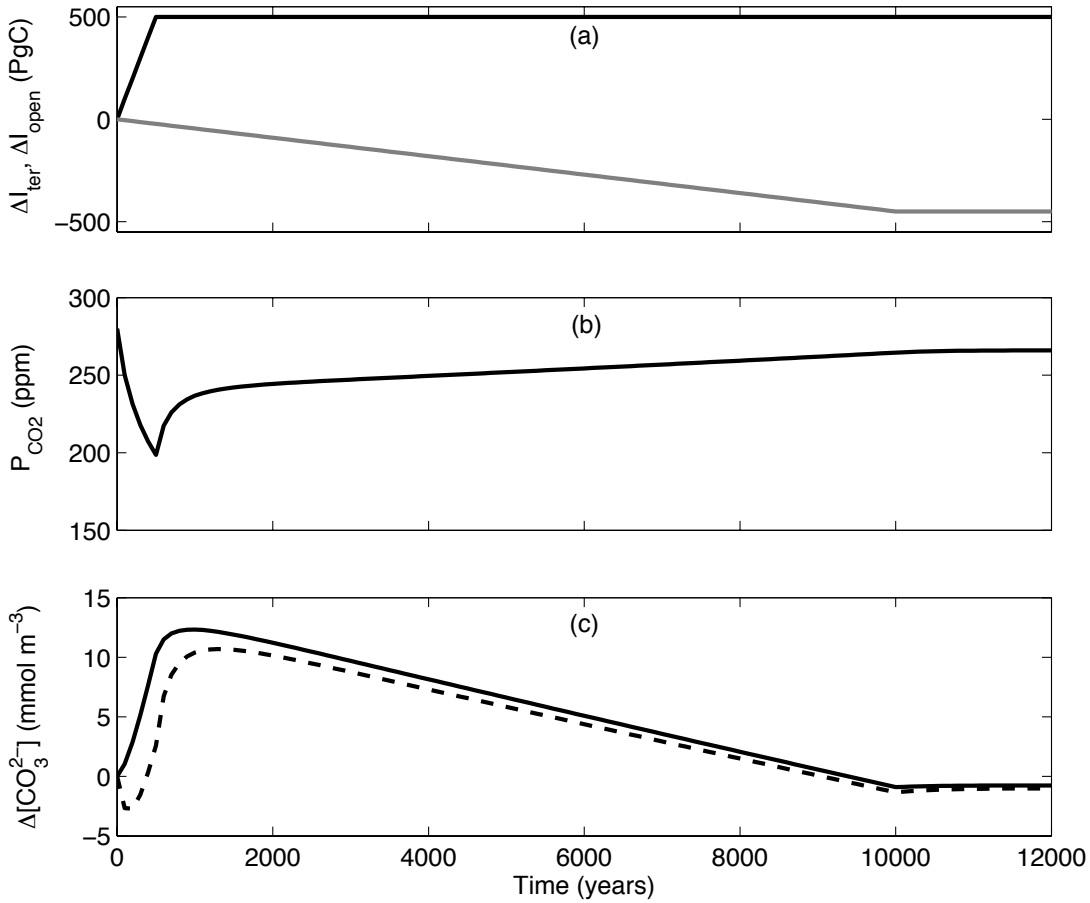

743
744
745 Figure 8: Time evolution of P_{CO2} and global mean $[CO_3^{2-}]$ in the Isopycnal Box Model and
746 the theoretical prediction following prescribed perturbations to ΔI_{ter} and ΔI_{open}. (a) Prescribed
747 temporal perturbations to ΔI_{ter} (black) and ΔI_{open} (grey) over time. (b) Modelled P_{CO2} over
748 time. (c) Global mean $[CO_3^{2-}]$ over time from Isopycnal Box Model output (black solid line)
749 and predicted from theory (18) (black dashed line).
750

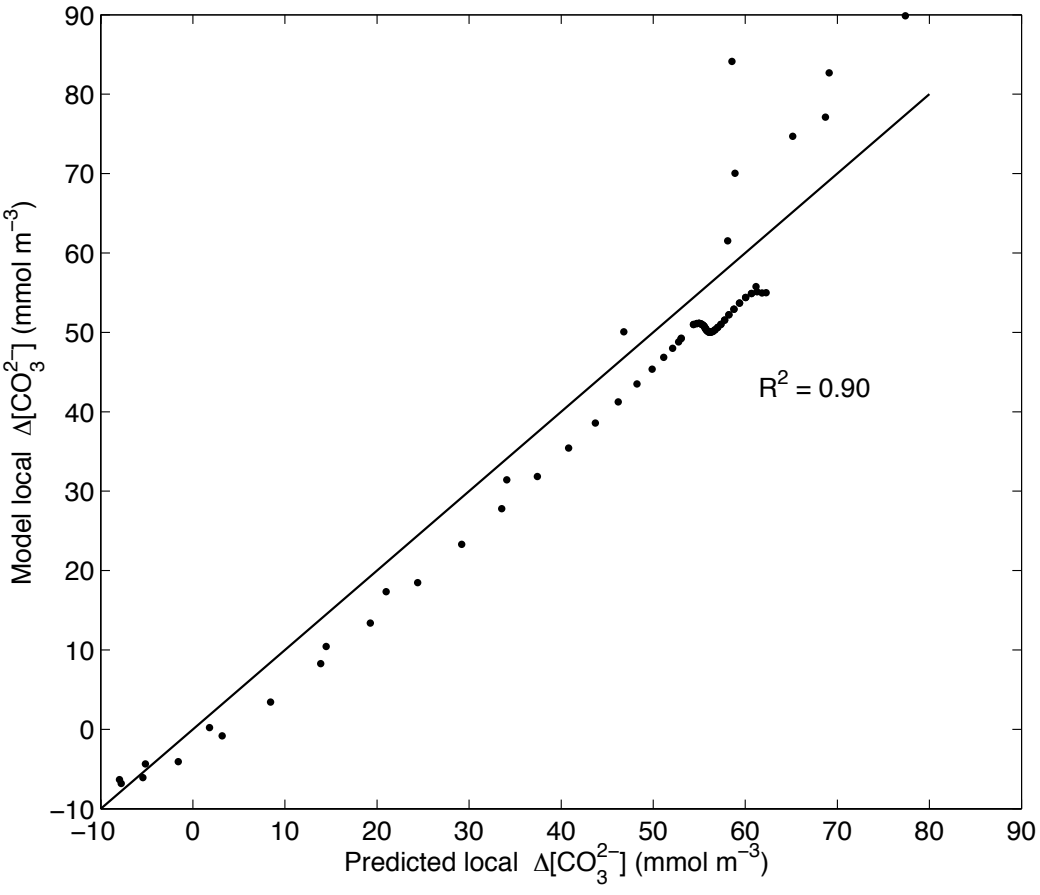

751
752
753 Figure 9: Modelled versus predicted (19) temporal variations in local $[CO_3^{2-}]$ between two
754 states of the Isopycnal Box Model. Dots indicate the results for individual boxes, and the
755 solid line indicates where the dots would be if the modelled and predicted $\Delta[CO_3^{2-}]$, (21)
756 were in perfect agreement. In the initial state $\overline{A_T}$ =2350 mmol m^{-3}, P_{CO2} = 280 ppm and
757 surface restored phosphate is 1.0 mmol m^{-3}. In the final state $\overline{A_T}$ =2500 mmol m^{-3}, P_{CO2} = 180
758 ppm and surface restored phosphate is 0.25 mmol m^{-3}.
759